International Journal of Microwave and Wireless Technologies

cambridge.org/mrf

Design and optimization of dual-band CSRR sensor for material characterization

Ali Zolfagharian and Fatemeh Geran

Department of Electrical Engineering, Shahid Rajaee Teacher Training University, Tehran, Iran

Research Article

Cite this article: Zolfagharian A, Geran F (2026) Design and optimization of dual-band CSRR sensor for material characterization. *International Journal of Microwave and Wireless Technologies* **18**(4), 618–624. https://doi.org/10.1017/S1759078726103705

Received: 6 July 2025 UTC
Revised: 29 June 2026 UTC
Accepted: 30 June 2026 UTC
First published online: 11 September 2026 UTC

Keywords
CSRR; metamaterial sensor; material characterization; dual-band sensor; microwave sensor

Corresponding author: Ali Zolfagharian; Email: ali.zolfagharian76@gmail.com

Abstract

The analysis of materials plays a critical role in ensuring product quality, driving innovation, improving cost-effectiveness, and maintaining safety standards across a wide range of industries. An effective method for material characterization involves evaluating permittivity using sensors based on metamaterials, which are renowned for their ability to provide fast and accurate results. A new sensor, the dual-band octagonal Complementary Split Ring Resonator, has been developed using metamaterial technology to measure the dielectric properties of materials. This sensor is fabricated on an affordable FR4 substrate with a 50 Ω microstrip line and has undergone testing with various materials to improve its quality factor and sensitivity. Noteworthy is the sensor's consistent performance even when analyzing materials that slightly exceed the designated measurement threshold. The unloaded S21 response shows depths of −25 dB for the first notch and −38 dB for the following notch. Furthermore, the research also presents findings from various configurations of the measurement under test under different load conditions.

Introduction

Metamaterial-based sensors are increasingly preferred for a wide range of sensing applications in fields such as biomedical, electrical, chemical, industrial, food quality assessment, and agriculture [1, 2]. These sensors are valued for their enhanced sensitivity, high-quality factor, simple manufacturing process, and cost-effectiveness [2]. The evaluation of materials can be effectively carried out by analyzing their permittivity, with metamaterial-based sensors serving as a practical tool for this purpose [3]. The determination of a material's electric permittivity can be achieved by studying the S-parameters of the sensor [4]. A novel sensor utilizing metamaterials has been specifically developed for this purpose.

Metamaterials were initially introduced by Veselago in 1968, and the Metamaterial-based split ring resonator (SRR) structure was pioneered by Pendry et al. in 1999 [5]. This study utilizes the Complementary Split Ring Resonator (CSRR), which is essentially the inverse of the SRR pattern etched onto the ground plane. The preference for CSRR over SRR is attributed to its higher sensitivity compared to SRR [6]. Previous studies have demonstrated that CSRR outperforms SRR in terms of sensitivity when both structures have equivalent dimensions [2]. Furthermore, the broader fringing electric fields generated by CSRRs, as opposed to SRRs, facilitate the determination of dielectric properties of larger samples [2]. Placing the material under test (MUT) on the ground plane induces a shift in the resonance frequency, enabling the calculation of the MUT's permittivity based on the sensor's resonance frequency with the MUT.

Various metamaterial configurations have been developed for diverse applications, with rectangular and circular shapes being particularly common. Through sensitivity analysis, it has been determined that circular sensors exhibit greater responsiveness to changes in the permittivity of the MUT [7] compared to rectangular sensors of equivalent area [8]. Additionally, circular CSRR structures are anticipated to have a higher resonant frequency than their rectangular counterparts for the same unit cell area [9]. The depth of the notch in the S-parameter output is a crucial factor in ensuring accurate measurements. A deeper notch and a higher Q-factor indicate improved sensor precision. A comparative evaluation of sensor performance based on the depth of the notch is presented in Table 1. In the pursuit of developing an innovative metamaterial shape, an octagonal design has been chosen. Following numerous simulations conducted using CST Studio Suite, the final sensor configuration is illustrated in Fig. 1(b).

This sensor is specifically engineered to function on two separate frequency bands. Utilizing multiband sensing serves to improve the reliability of sensing by offering sensors that possess high sensitivity and quality factors. Furthermore, variations in frequency shifts may result in identical outcomes for different mixtures; therefore, measurements conducted at a constant frequency are only capable of distinguishing chemicals based on this shift, thereby constraining the accuracy of identification [10].

© The Author(s), 2026. Published by Cambridge University Press in association with The European Microwave Association.

Table 1. Different sensor patterns comparison based on depth notch

Reference	Resonator topology	Absorption band	Resonator pattern	Resonant frequency (f_0)	S21 notch depth without MUT
[4]	Circular CSRR	Single		6.01 GHz	−31.157 dB
[11]	Circular CSRR	Multiple		2.45 GHz	≈−22 dB
				3.8 GHz	≈−28 dB
				5.8 GHz	≈−30 dB
[12]	Rectangular SRR	Single		2.1 GHz	≈−11 dB
[1]	Rectangular CSRR (microfluidic)	Single		2.02 GHz	−24 dB
[13]	S-shape resonator	Single		1.8 GHz	≈−13 dB
[14]	CSSRR	Dual		5.35 GHz	−62.08 dB
				8.06 GHz	−19.06 dB
[15]	CSRR	Single		2.461 GHz	−27 dB
This work	Octagonal CSRR	Dual		2.37 GHz	−25 dB
				4.88 GHz	−38 dB

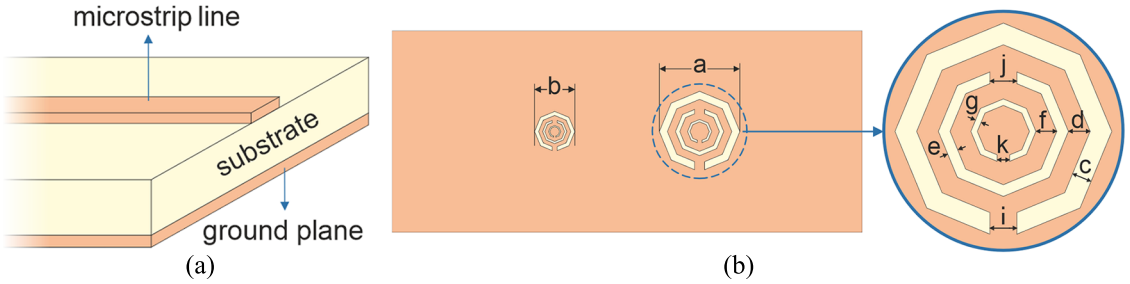


Figure 1. (a) Layers of sensor. (b) Designed sensor with parameters.

Sensor design

Based on previous studies, circular CSRR sensors demonstrate a deeper resonance notch compared to their rectangular counterparts. However, structures with sharp edges exhibit stronger localized electric fields around these regions, resulting in enhanced sensitivity. Therefore, in this work, an octagonal CSRR sensor is proposed to combine the advantage of the circular geometry with the enhanced field localization associated with sharp-edged structures [16].

The design was intentionally optimized to produce a deeper transmission notch because a larger notch increases the fraction of energy captured by the resonator's near-field and improves the measurability of the resonance. This yields more pronounced, repeatable resonance peaks with higher frequency-shift sensitivity and better signal-to-noise for extracting the resonant frequency used in the characteristic equation, which in turn improves the accuracy and resolution of the dielectric-constant measurement [17].

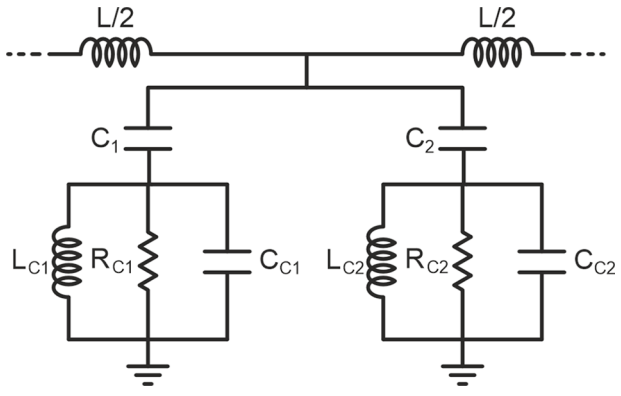


Figure 2. Equivalent circuit model of the CSRR sensor.

To enhance the performance of the proposed sensor, an optimization process was conducted to achieve an optimal balance among sensitivity, compactness, and fabrication feasibility. In the

https://doi.org/10.1017/S1759078726103705 Published online by Cambridge University Press

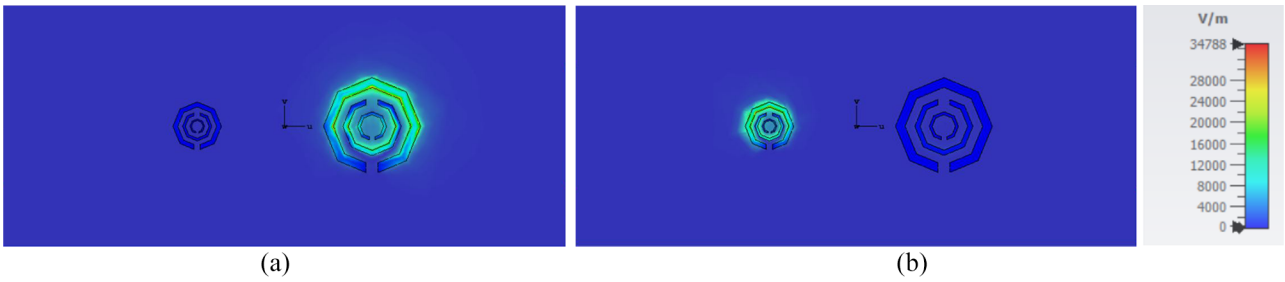


Figure 3. (a) Electric field on the ground plane at 2.37 GHz. (b) Electric field on the ground plane at 4.88 GHz.

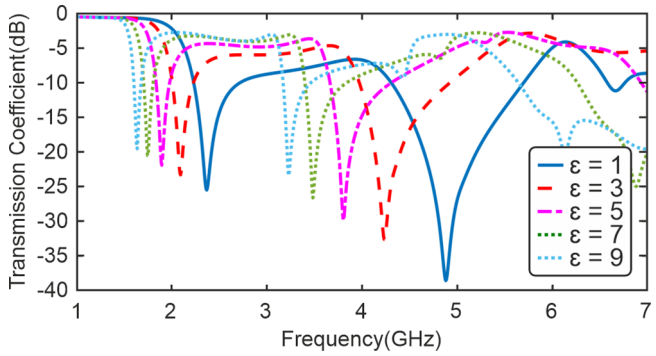


Figure 4. Simulated transmission response of the sensor in different permittivities.

first stage, a single-resonance CSRR sensor was designed, and a series of parametric sweeps were performed on the critical geometrical parameters, including the split-gap width, number of rings, ring spacing, and conductor line width. After determining the configuration that provided the highest sensitivity and the deepest resonance notch, a second resonant structure was incorporated into the design. Subsequently, additional parametric sweeps were carried out on the inter-structure spacing to finalize the optimized sensor geometry.

To obtain optimal resonator geometry with maximum sensitivity, the design process started from a single octagonal resonator incorporating a notch. First, the notch position along the octagonal contour was systematically evaluated in CST Studio Suite to maximize the resonance frequency shift induced by the dielectric under test, while maintaining a well-defined transmission notch in the S_{21} response. After selecting the best notch location, two additional parameters—the octagon linewidth and the notch width—were swept to determine the primary sensor geometry. These parameters directly influence the effective inductance and capacitance of the resonator and therefore control the resonance frequency, notch bandwidth, and quality factor.

To further enhance field confinement and increase the interaction region between the resonator and the MUT, a second octagonal structure, similar to the first but scaled in size, was added to the design. A parametric sweep was then performed to determine the optimum scaling factor and spacing between the two octagonal elements. To further improve sensitivity, a third scaled octagonal element was introduced and optimized using the same procedure.

In addition to linewidth, notch dimensions, and spacing between the octagonal elements, the relative rotation angle between the octagonal structures was found to significantly affect the coupling strength and the resulting S_{21} notch characteristics. The best response was obtained when the second octagon was rotated by 180° relative to the other elements, as shown in Fig. 1(b). The same optimization procedure was then applied to the third octagonal element. During the entire optimization procedure, the quality factor was evaluated in order to ensure high sensitivity and is defined as:

$$Q = \frac{f_r}{\mathrm{BW}_{-3\mathrm{dB}}} \tag{1}$$

where f_r is the resonance frequency, and $\mathrm{BW}_{-3\mathrm{dB}}$ is the −3 dB bandwidth around the resonance.

After obtaining the final resonator geometry, a second resonator was added on the ground plane. The distance between the two resonators was then swept to achieve high sensitivity while preserving a clear and measurable transmission notch. This step is critical because coupling between the two resonators modifies the resonance behavior and can significantly affect both the resonance frequency shift and the overall sensor performance.

The frequency range of 2–10 GHz was selected for this sensor, as it offers good sensitivity while being less susceptible to electromagnetic noise. Moreover, since the inner octagonal section of the smaller resonator is relatively thin, reducing its dimensions excessively would increase fabrication complexity and cost. Therefore, the chosen frequency band represents a suitable compromise between performance, manufacturability, and measurement stability.

The sensor is implemented on a microstrip, as depicted in Fig. 1(a): a trace line on the top, a substrate layer, and a ground plane with metamaterial-inspired shapes etched onto it. The substrate is constructed from low-cost FR4 with a thickness of 0.8 mm, while the two additional layers are made of 0.035 mm copper. The substrate has a length of 70 mm and a width of 30 mm. Additionally, the dimensions are specified as follows: $a = 12$ mm, $b = 6$ mm, $c = d = f = 3$ mm, $e = 1.6$ mm, $g = 0.9$ mm, $i = j = 4$ mm, and $k = 1.9$ mm, and the smaller resonator shape has dimensions exactly half of the larger one. The resonant frequencies of the sensor are 4.88 GHz and 2.37 GHz.

An equivalent circuit model was developed to provide physical insight into the resonance mechanism of the proposed sensor and to support the design and optimization procedure. In the proposed circuit, the two transmission notches observed in the S_{21} response are represented by two resistor-inductor-capacitor (RLC) resonant branches, where each RLC branch corresponds to one resonant element (or resonance mode) of the sensor structure. The inductance and capacitance values model the effective current path and electric-field concentration of the resonators, while the resistive terms account for conductor and dielectric losses. The coupling between the microstrip line and the resonators is modeled through coupling capacitances, which mainly determine the notch depth

https://doi.org/10.1017/S1759078726103705 Published online by Cambridge University Press

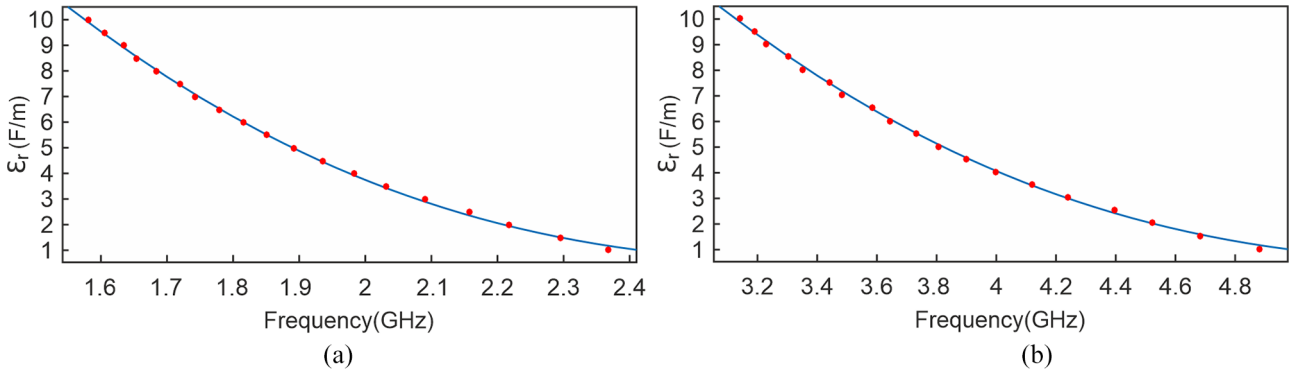


Figure 5. (a) Fitted curve to larger resonator's simulation data. (b) Fitted curve to smaller resonator's simulation data.

and bandwidth. This circuit model provides a compact representation that enables interpretation of the main geometrical parameters (notch width, linewidth, spacing, and rotation angle) in terms of effective circuit parameters and allows direct validation against full-wave CST results.

Figure 2 illustrates the equivalent circuit of the proposed sensor [18].

Simulation

At the resonance of the CSRR, significant fringing electric fields are generated in the ground plane, providing an additional method to determine dielectric properties [19]. The electromagnetic energy, concentrated in a confined area near the substrate at the resonant frequency, is used to determine dielectric properties [20]. The most intense electric field is established between the microstrip line and the ground plane. As shown in Fig. 3, the concentration of the electric field near each resonator results in the formation of notches in the transmission coefficient plot at the resonant frequency. The positioning of the MUT can be more accurately determined by pinpointing the location of the strong electric field. Placing the MUT on the sensor causes a shift in these notches. The transmission coefficient is depicted in Fig. 4 for various MUTs with differing permittivity. The shift of the notch from $\varepsilon_r = 1$ to $\varepsilon_r = 3$ is 640 MHz for the smaller resonator with a resonant frequency of 4.88 GHz, demonstrating the high sensitivity of the sensor. Additionally, the quality factor for the 4.88 GHz band is 81.3, signifying a remarkable quality factor for a sensor employing an FR4 substrate. Furthermore, the frequency shift for the larger resonator with the same values of ε_r is 277 MHz, and the Q-factor is equal to 41.5 dB.

As illustrated in Fig. 4, an increase in ε causes a reduction in notch depth. Moreover, to prevent band interference, a specific range of permittivity should be selected for measurement. Therefore, an ε_r of less than 10 should be chosen.

Temperature is another parameter that can influence this observation and cause variations in the results. Temperature rise results in an increase in the permittivity of FR4 [21, 22], which causes variations in the resonance frequency and decreases the accuracy of the sensor. Therefore, all measurements should be obtained at a constant temperature. With additional simulations involving different MUTs, a relationship between permittivity and frequency can be derived. A polynomial function is considered to fit the simulation data:

$$\varepsilon_r = A_1 f^2 + A_2 f + A_3 \quad (2)$$

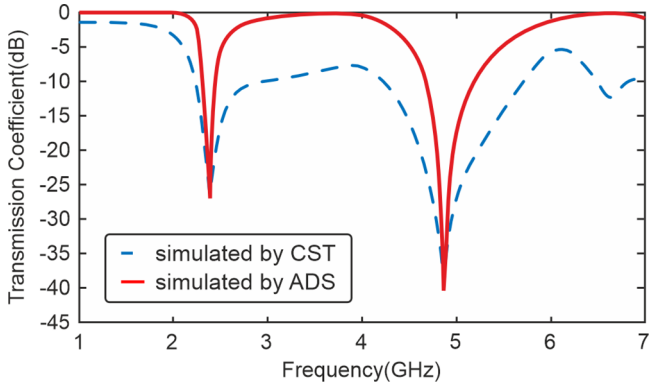


Figure 6. Comparison of the transmission coefficient $|S_{21}|$ obtained from full-wave CST simulation and the proposed equivalent circuit model simulated in ADS.

Table 2. Equivalent circuit parameters of the sensor

Parameter	Value	Unit
L	4.2	nH
C_1	0.5989	pF
L_{c1}	3.0	nH
C_{c1}	0.9042	pF
R_{c1}	7.0	kΩ
C_2	0.43822	pF
L_{c2}	0.8	nH
C_{c2}	0.890	pF
R_{c2}	7.0	kΩ

Simulation data are processed in MATLAB, yielding a quadratic equation for each resonator.

The resonance frequency decreases as the dielectric constant increases. This behavior is expected, since the MUT increases the effective capacitance of the CSRR structure, thereby reducing the resonance frequency according to the inductance-capacitance (LC) resonance principle.

In Fig. 5, the quadratic equation fitted to the simulation data is illustrated. For the larger resonator with 2.37 GHz resonant frequency, the coefficients are A1 = 9.404, A2 = −48.2, and A3 = 62.57, while for the smaller resonator, the coefficients are A1 = 2.001, A2 = −21.05, and A3 = 56.21.

https://doi.org/10.1017/S1759078726103705 Published online by Cambridge University Press

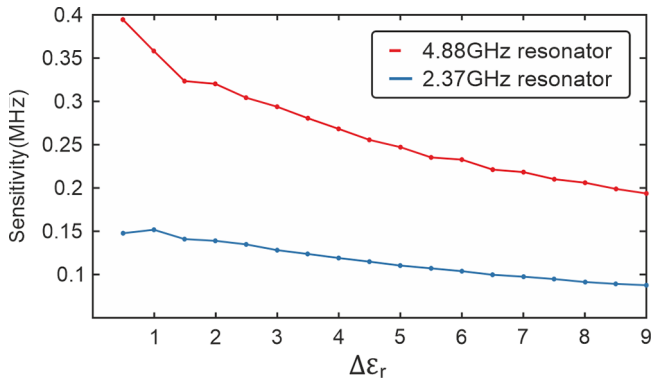


Figure 7. Calculated sensitivity of each band versus relative permittivity variation (ε_r).

To validate the proposed equivalent circuit model, the transmission coefficient obtained from the circuit simulation in Advanced Design System (ADS) is compared with the full-wave electromagnetic simulation performed in CST Studio Suite, as shown in Fig. 6. The equivalent circuit successfully reproduces the two resonance notches and accurately predicts the resonance frequencies at 2.37 GHz and 4.88 GHz, in excellent agreement with the CST results. The extracted lumped-element values used in the circuit model are summarized in Table 2 and were obtained by fitting the ADS response to the CST $|S_{21}|$ curve, where the RLC parameters were adjusted to match the resonance frequencies and bandwidth, while the coupling capacitances were tuned to reproduce the notch depth. Minor differences in notch depth and out-of-resonance behavior can be attributed to higher-order parasitic effects, radiation, and distributed coupling mechanisms that are inherently captured in the full-wave simulation but are not fully represented in the lumped-element circuit model. Overall, the comparison confirms that the proposed circuit model provides an accurate representation of the sensor resonance behavior and can be used to support the design analysis.

To evaluate the sensing performance, a sensitivity analysis was carried out by investigating the resonance frequency variation of the proposed CSRR sensor when different dielectric materials were placed on the sensitive region. The sensitivity is defined as the change in resonance frequency with respect to the variation in the relative permittivity of the MUT, and it is expressed as:

$$Sensitivity = \frac{\Delta f}{\Delta \varepsilon_r} \tag{3}$$

where $\Delta f_r = f_{r0} - f_r$ is the resonance frequency shift, f_{r0} is the resonance frequency corresponding to the reference condition (no load), and f_r is the resonance frequency in the presence of the MUT. $\Delta \varepsilon_r$ represents the relative permittivity change between two consecutive MUT cases. A higher sensitivity indicates that smaller variations in dielectric properties can be detected.

The sensitivity corresponding to selected permittivity values within the investigated range was computed using (3), and the results are reported in Fig. 7.

Fabrication and measurement

The sensor was constructed according to the specifications provided in the sensor design section, with the impedance of the microstrip line standardized at 50 Ω. Figure 8(a) depicts the experimental setup, illustrating the sensor's connection to a network analyzer. Furthermore, Fig. 8(b) displays the ground plane of the manufactured sensor.

The dimensions of the MUT play a crucial role in ensuring the accuracy of measurements. When the MUT sufficiently covers the area surrounding the resonators, the outcomes are relatively consistent. However, for enhanced precision, it is recommended to maintain uniform measurements. These measurements were obtained through simulations involving various MUT sizes, which were reflected in both the simulation outcomes and the practical measurements. In this particular measurement, the MUT dimensions were set at 60 × 20 × 3 mm. Consistent environmental conditions are essential to ensure accurate results and prevent interference with the field distribution around the test probe during measurements [3]. Figure 9 illustrates the output from the network analyzer, highlighting the alignment between simulation and measurement results. The frequencies obtained from the measurements were incorporated into the formula derived from simulations, and the results are outlined in Table 3.

The imaginary part of permittivity can also be derived from the loss tangent. To calculate the loss tangent, the quality factor must first be determined, as given by:

$$\frac{1}{Q_L} + \frac{1}{Q_0} = \tan\delta \tag{4}$$

Where Q_0 and Q_L signify the quality factors of the sensor without and with the sample. ε'' is calculated using the following equation:

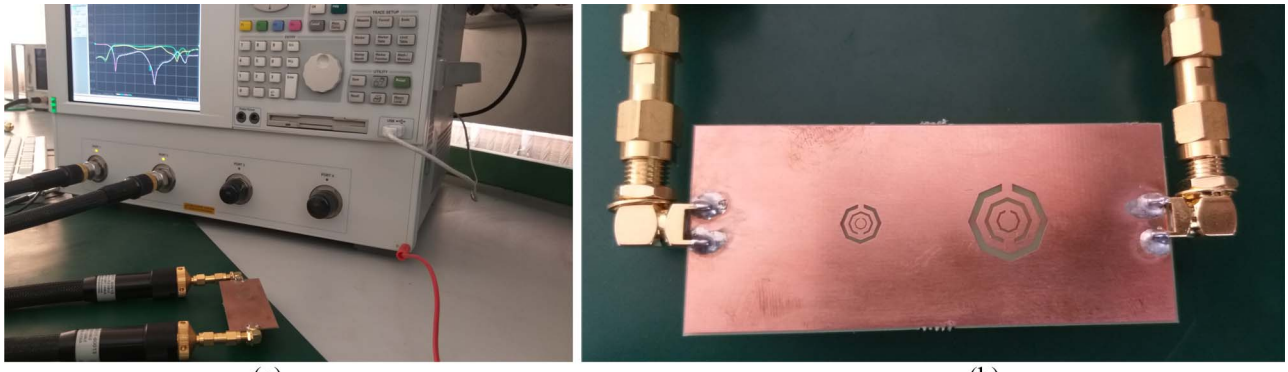


Figure 8. (a) Fabricated sensor connected to network analyzer. (b) Fabricated sensor top view.

https://doi.org/10.1017/S1759078726103705 Published online by Cambridge University Press

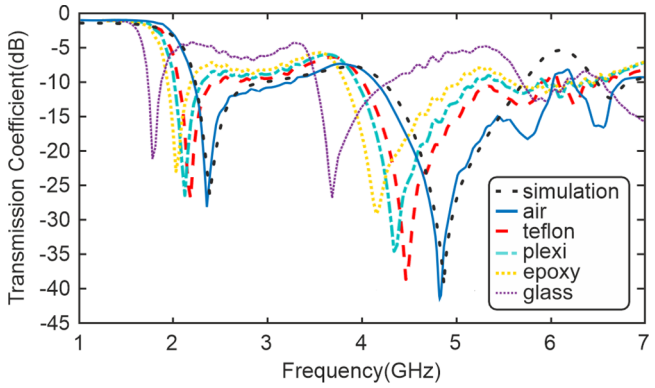


Figure 9. Measurement results of the fabricated sensor with different MUTs.

Table 3. Measured relative permittivity values

MUT	$\varepsilon_{r,R}$	$\varepsilon_{r,M1}$	$Error_{M1(\%)}$	$\varepsilon_{r,M2}$	$Error_{M2}$
Teflon	2.10 [23, 24]	2.073	0.01	2.221	0.05
Plexi	2.60 [23, 24]	2.524	0.03	2.577	0.01
Epoxy	3 [25, 26]	3.288	0.09	3.397	0.13
Glass	6.07 [3]	5.819	0.04	6.525	0.07

*$\varepsilon_{r,R}$ is reference value of dielectric constant; $\varepsilon_{r,M1}$ and $\varepsilon_{r,M2}$ represent measured permittivity of smaller and larger resonator; $Error_{M1}$ and $Error_{M2}$ represent error of measurements

Table 4. Measured loss tangent and imaginary part of permittivity values*

MUT	$\tan\delta_{,M1}$	$\varepsilon'',_{M1}$	$\tan\delta_{,M2}$	$\varepsilon'',_{M2}$
Teflon	0.00033	0.000684	0.00039	0.000866
Plexi	0.0088	0.0222	0.0096	0.0247
Epoxy	0.00787	0.0258	0.01152	0.0267
Glass	0.00560	0.0325	0.00546	0.0356

The ε' can be used for materials with similar permittivity constants. For similar permittivity constants, ε' can be used for more accurate material identification.

$$\varepsilon'' = \varepsilon_r \cdot \tan\delta \tag{5}$$

Where ε_r is derived from the measured data of the sensor. The ε'' values for both resonators are shown in Table 4.

Conclusion

An effective microwave sensor was developed, modeled, produced, and evaluated for material analysis purposes. Following an examination of various sensor configurations, a dual-band octagonal CSRR was devised. The experimental findings closely matched the results obtained through simulation. The sensor demonstrated high sensitivity and a notable notch depth of −38 dB for the smaller resonator and −25 dB for the larger resonator, which is considered impressive considering the utilization of an FR4 substrate. A polynomial function was derived to describe the correlation between the sensor's permittivity and frequency. The results demonstrate that the proposed CSRR sensor provides a consistent and measurable frequency shift for different dielectric materials. The frequency shift exhibits a monotonic dependence on the permittivity, confirming that the sensor can distinguish materials with different dielectric constants.

Acknowledgements. This work is supported in part by Shahid Rajaee Teacher Training University.

Competing interests. The authors have no competing interests to declare that are relevant to the content of this article.

References

1. **Ebrahimi A, Withayachumnankul W, Al-sarawi S and Abbott D** (2014) High-Sensitivity Metamaterial-Inspired Sensor for Microfluidic Dielectric Characterization. *IEEE Sensors Journal* **14**, 1345–1351. https://doi.org/10.1109/JSEN.2013.2295312.
2. **Prakash D and Gupta N** (2022) Applications of metamaterial sensors: A review. *International Journal of Microwave and Wireless Technologies* **14**, 19–33. https://doi.org/10.1017/S1759078721000039.
3. **Chakyar SP, Simon K, Bindu S, Andrews J and Joseph VP** (2017) Complex permittivity measurement using metamaterial split ring resonators. *Journal of Applied Physics* **121**, 054101. https://doi.org/10.1063/1.4975111
4. **Shahzad W, Hu WD, Samad A and Ligthart LP** (2020) Complementary Split Ring Resonator based Metamaterial sensor for Dielectric Materials Measurements. *17th International Bhurban Conference on Applied Sciences and Technology*. Islamabad.
5. **Pendry JB, Holden AJ, Robbins DJ and Stewart WJ** (1999) Magnetism from conductors and enhanced nonlinear phenomena. *IEEE Transactions on Microwave Theory and Techniques* **47**, 2075–2084. https://doi.org/10.1109/22.798002.
6. **Albishi AM, Mirjahanmardi SH, Ali AM, Nayyeri V, Wasly SM and Ramahi** (2019) O.M.: Intelligent sensing using multiple sensors for material characterization. *Sensors* **19**, 4766. https://doi.org/10.3390/s19214766.
7. **Govind G, Tiwari N, Agrawal K and Akhtar MJ** (2018) Microwave subsurface imaging of composite structures using complementary split ring resonators. *IEEE Sensors Journal* **18**, 7442–7449. https://doi.org/10.1109/JSEN.2018.2859228.
8. **Ansari MAH, Jha AK and Akhtar MJ** (2015) Design and application of the CSRR-based planar sensor for noninvasive measurement of complex permittivity. *IEEE Sensors Journal* **15**, 7181–7189. https://doi.org/10.1109/JSEN.2015.2469683.
9. **Boybay MS and Ramahi** (2012) O.M.: Material characterization using complementary split-ring resonators. *IEEE Transactions on Instrumentation and Measurement* **61**, 3039–3046. https://doi.org/10.1109/TIM.2012.2203450.
10. **Zhou H, Hu D, Yang C, Chen C, Ji J, Chen M, Chen Y, Yang Y and Mu X** (2018) Multi-band sensing for dielectric property of chemicals using metamaterial integrated microfluidic sensor. *Scientific Reports* **33**, 2253–2267.
11. **Ansari MAH, Jha AK, Akhter Z and Akhtar MJ** (2018) Multi-band RF planar sensor using complementary split ring resonator for testing of dielectric materials. *IEEE Sensors Journal* **18**, 6596–6606. https://doi.org/10.1109/JSEN.2018.2822877.
12. **Ebrahimi A, Scott J and Ghorbani K** (2018) Differential sensors using microstrip lines loaded with two split-ring resonators. *IEEE Sensors Journal* **18**, 5786–5793. https://doi.org/10.1109/JSEN.2018.2840691.
13. **Sabah C and Nesimoglu T** (2016) Design and characterization of a resonator-based metamaterial and its sensor application using microstrip technology. *Optical Engineering* **55**, 027107.
14. **Haq TU, Ruan C, Wang R and Wu T** (2018) High Q dual band super high frequency notch filter based on complementary metamaterial. *Progress in Electromagnetics Research Symposium*. Toyama.
15. **Saadat SM, Nayyeri V, Khanjarian M, Soleimani M and Ramahi O** (2019) A CSRR-based sensor for full characterization of magneto-dielectric materials. *IEEE Transactions on Microwave Theory and Techniques* **67**, 806–814. https://doi.org/10.1109/TMTT.2018.2882826.
16. **Haq T and Koziel S** (2023) Rapid design optimization and calibration of microwave sensors based on equivalent complementary resonators for high sensitivity and low fabrication tolerance. *Sensors* **23**. https://doi.org/10.3390/s23021044

17. **Shahzad W, Hu W, Ali Q, Raza H, Abbas SM and Ligthart LP** (2022) A low-cost metamaterial sensor based on ds-csrr for material characterization applications. *Sensors* **22**. https://doi.org/10.3390/s22052000
18. **Baena JD, Bonache J, Martin F, Sillero RM, Falcone F, Lopetegi T Laso MA, Garcia-Garcia J, Gil I, Portillo MF and Sorolla M** (2005) Equivalent-circuit models for split-ring resonators and complementary split-ring resonators coupled to planar transmission lines. *IEEE Transactions on Microwave Theory and Techniques* **53**, 1451–1461. https://doi.org/10.1109/TMTT.2005.845211
19. **Lee CS and Yang CL** (2014) Complementary split-ring resonators for measuring dielectric constants and loss tangents. *IEEE Microwave and Wireless Components Letters* **24**, 563–565.
20. **Lim S, Kim CY and Hong S** (2018) Simultaneous measurement of thickness and permittivity by means of the resonant frequency fitting of a microstrip line ring resonator. *IEEE Microwave and Wireless Components Letters* **28**, 539–541.
21. **Paghi A, Trupiano G, Puglia C, Burgaud H, De Simoni G, Greco A and Giazotto F** (2024) Estimation of the FR4 microwave dielectric properties at cryogenic temperature for quantum-chip-interface PCBs design. *IEEE Transactions on Instrumentation and Measurement* **73**, 1–7. https://doi.org/10.1109/TIM.2024.3372217.
22. **Miller P**: A tale of four substrates-EMI and thermal comparisons of different PCB materials, 10th International Conference on Electromagnetic Compatibility, Coventry, 1997.
23. **Tiwari NK, Tiwari Y and Akhtar MJ** (2018) Design of CSRR-based electronically tunable compact RF sensor for material testing. *IEEE Sensors Journal* **18**, 7450–7457. https://doi.org/10.1109/JSEN.2018.2861365.
24. **Shafi MKT, Ansari MAH, Jha AK and Akhtar MJ** (2017) Design of SRR-based microwave sensor for characterization of magnetodielectric substrates. *IEEE Microwave and Wireless Components Letters* **27**, 524–526.
25. **Yasir M, Savi P, Yahya MH, Giorcelli M and Tagliaferro A** (2014) Wide band characterization of MWCNTs Composites based on epoxy resin: Complex permittivity and shielding effectiveness, *Proceedings of 2014 Mediterranean Microwave Symposium*. Marrakech.
26. **Hasan N, Hussain NSM, Faudzi AAM, Shaharum SM, Yusof NAT, Noordin NH, Mohtadzar NAA and Karim MSA** (2019) Cured epoxy resin dielectric characterization based on accurate waveguide technique, *5th International Conference on Green Design and Manufacture*. Jawa Barat.



Ali Zolfagharian was born in Tehran, Iran, in 1997. He received his B.Sc. degree in Electrical Engineering from Shahid Rajaee Teacher Training University, Tehran, Iran, in 2020. He is currently working as an electrical engineer specializing in the optimization of energy systems and uninterruptible power supplies (UPS).



Fateme Geran was born in Qaem Shahr, Iran, in 1977. She received her BSc degree in Electrical Engineering (Telecommunication) from Tehran University, Tehran, Iran, in 1999. Also, she received her MSc and PhD degrees in Electrical Engineering (Telecommunication) from Tarbiat Modares University, Tehran, Iran, in 2003 and 2009, respectively. She is currently an assistant professor in the Faculty of Electrical Engineering at Shahid Rajaee Teacher Training University, Tehran, Iran. Her research interest fields are antenna, RF subsystems in microwave and mm-wave Bands and RF energy harvesting.

https://doi.org/10.1017/S1759078726103705 Published online by Cambridge University Press